USE OF EARTH OBSERVATION DATA FOR HYDRODYNAMIC MODELLING IN THE MARA WETLANDS

Joseph O.D. Mtamba [1,2], Rogier van der Velde [2], Preksedis M. Ndomba [1], Verkedy, Zoltan [2], Felix W. Mtalo [1] and Alessandra Crosato [3]

(1) Department of Water Resources Engineering, P.O Box 35131, University of Dar es Salaam, P.O Box 35131 Dar es Salaam, Tanzania. joseph.mtamba@udsm.ac.tz, pmndomba@uccmail.co.tz, mtalo@wrep.udsm.ac.tz,

(2) Faculty of Geo-Information and Earth Observation , University of Twente-ITC, P.O Box 217, 7500 AE, Enschede, The Netherlands. j.o.d.mtamba@utwente.nl, r.vendervelde@utwente.nl, z.verkerdy@utwente.nl

(3) Department of Water Science and Engineering , UNESCO –IHE, P.O Box 3015, 2601 DA, Delft, The Netherlands. a.crosato@unesco-ihe.org

ABSTRACT

Vegetation characteristics can not only be used to derive spatial hydrodynamic roughness parameters but also to correct vegetation artefacts in freely downloadable Digital Elevation Models for hydrodynamic modelling. An exponential backscattering model for vegetation canopy height model was developed using standard deviation of cross polarization backscatter coefficient of Radarsat-2 SAR wide swath mode and in situ vegetation height data. The retrieved spatial vegetation height was used to correct vegetation artefacts in freely downloadable Advanced Spaceborne Thermal Emission and Reflectance Radiometer Global Digital Elevation Model (ASTERDEM) released in 2011. The relative spatial hydrodynamic roughness within a vegetation class was derived from cross polarization ratio. Preliminary results show that the accuracy of ASTERDEM improved the elevation estimates by root mean square error from 5.1 m to 3.0m. Simulation results using Earth Observation (EO) data for calibration and validation using an internal gauging station yielded promising Nash - Sutcliffe efficiency criterion of 0.38 and 0.45. The results shows that if high resolution DEM is available, spatial roughness parametrization using cross-polarization ratio of Synthetic Aperture Radar (SAR) imagery may be useful in modelling extensive floodplains where optimization of roughness parameter is not necessary due to computational limitations.

Key words: Backscattering coefficient, canopy height model, flood modelling, surface roughness

1.0 INTRODUCTION

Mara wetlands is characterized by flooding annually. The origin of floods is mostly from rainfall generated surface runoff from the Mara basin catchment. Climate change and land use alteraton has been globally advocated to be major causes of floods which results to alteration of river hydraulic regime. The alteration of river hydraulic regime not only affects the wetland ecosystems and processes [1] , but also Communities living along the river wetland. These local communities depend mostly on the services accrued from the riverine and riparian ecosystems which are always affected by floods[2]. The sustainability of these services is underpinned by a healthy ecosystem functioning. The communities around the wetland are impacted by frequent floods due to changes in quantity and quality of river flows in terms of flood damage ,health, income, food security, and natural resources [3].

The important role of flooding of in the Mara wetland is ecological one. The ecological aspect of flood is discussed as a concept of flood pulse by researchers[4]-[6], providing a floodplain with mineral content, substrates, moisture which creates condition for development of fluviogenous ecosystem in the Mara floodplain. The seasonal flooding promotes the exchange of materials and organisms among the complex mosaic of floodplain habitat. To predict the impacts on the wetland, the hydraulic processes of the Mara River including its floodplains have to be assessed at different temporal scales and spatial scale. The development of accurate and reliable numerical surface water flow model which well describes surface water flow on the wetland can be used as a tool to understand other hydrological processes and a wetland management tool.

One of the challenges and limitation of hydrodynamic modeling in the study is availability of topographic data. The influence of vegetation on accuracy of freely downloadable digital elevation model (DEM) need to be investigated and corrected. Flood modeling is more often interested on bare land surface that controls flood dynamics. Recently and highly accurate topographical data sets e.g. LIDAR (LIght Detection And Ranging of Laser Imaging Detection And Ranging) are preferred for flood inundation modeling with modern commercial 2/3D hydrodynamic models[7]-[12]. Unfortunately such data/information is not always readily available given time and budget constraints, therefore application of online freely downloadable DEMs may provide a quick reliable solution to understanding hydrological processes, flood flow dynamics and other ecological

processes on the earth's surface including wetlands.

This research evaluates application of EO data to support flood modelling for ecosystem study in Mara wetland where topographic and spatial roughness are not readily available. Radarsat 2 SAR imagery, Landsat 5 TM and ASTERDEM was used in this study to support parameterization of FLO-2D model.

2.0 STUDY AREA

The Mara wetlands (Fig.1) is one of the largest tropical wetland systems in East Africa and functions it receives flows from Mara river and releases into Lake Victoria. Mara river originates from hilly areas of Mau escarpment forest and passes through a vast low-lying areas across boarder national parks, its primary waterway running through the Serengeti national park. The flooding period occurs in the months of December/January or April/May and the flood depth varies with the flood volume varies, but typically averages may lie between 0.5 and 2 m in the flood plain. The riverbeds of the main Mara river and its tributaries are fairly well defined at their upper reaches, but become increasingly sinusoidal as they near the confluence of Tigithe river due to the low gradient across the plain. This results in decreased downstream river flow and increases sedimentation. This characteristic is common in most fluvial systems.

The figure below of the study area shows ten rain gauge stations in the Lower Mara basin with data of varying periods. 5 river gauged sites 1,2,3(5H2),4,5H3. Station 1-4 was used in previous study of rating curve development [13]. Station 5H2 and 5H3 are the Mara mine and Kirumi ferry gauge stations.

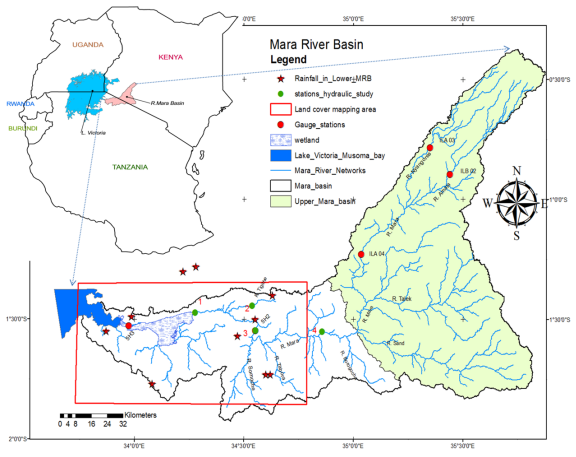

Figure 1. Study area

3.0 DATA

Data used in this study includes 12 Radarsat-2 images which were acquired in the Wide Swath mode with near range and far range incidence angle (θ) (W3, 38^{o} - 45^{0}) and the VH/VV polarization combination, Rainfall and flows data, in-situ vegetation height data, landsat vegetation classification map shape files (Mtamba et al., 2012)

3.1 Rainfall and flow data

The rainfall data from 10 gauge stations in the lower Mara basin was analysed and average aerial rainfall determined. The flows data at Mara mine (5H2) gauge station located at upstream of the wetland floodplain and rainfall were used to aid interpretation of SAR imagery. The two year flow hydrograph shows two distinct period of floods. November/December and April/May are flooding periods in the Mara wetlands. The floods are driven by excess rainfall as showed during flood peaks in Fig. 2 below.

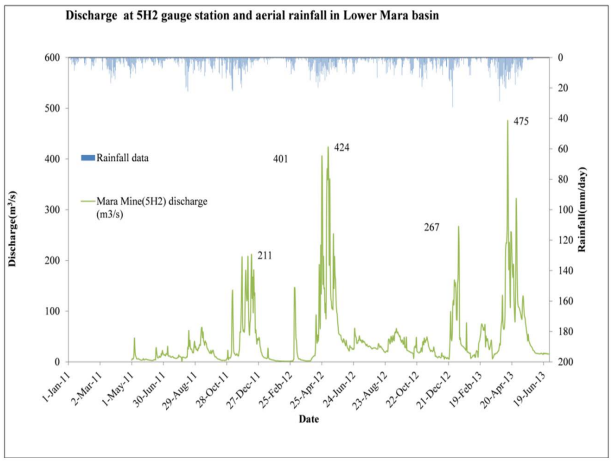

Figure 2. Rainfall and flows data

The rainfall data and flows were summarised to correspond with SAR data acquisition dates. The data shows there were five excess rainfall events that is likely to affect the quality of SAR backscattering coefficients.

Table 1. Summary of precedent flow and rainfall statistics

Date	Day Flow (m^3/s)	Monthly Flow (m^3/s)	Daily rainfall (mm)	Monthly rainfall (mm)
30.04.2011	8.5	20.0	14.3	113
24.05.2011	4.1	14.2	0.0	136
02.12.2011	145.3	135.5	8.6	264
26.12.2011	43.4	135.5	6.1	113
19.01.2012	5.2	14.0	0.0	35
07.03.2012	45.9	29.3	0.2	90
31.03.2012	2.2	29.3	4.6	53
24.04.2012	138.0	119.0	16.6	220
18.05.2012	145.3	221.0	21.2	214
11.06.2012	34.8	39.3	11.9	119

3.2 Radarsat 2 data

SAR data was obtained from RADARSAT-2 which was launched on 14th December 2007 by the Canadian Space Agency (CSA). Radarsat-2 carries a Synthetic Aperture Radar (SAR)RADARSAT-2 SAR operates at a frequency of 5.405 GHz (C-band). It that has been designed to satisfy commercial earth observation applications at a wavelength of 5.6 cm [14]. The system is capable of acquiring data is various imaging mode with fully polarimetric capability of producing multiple image products, including variable polarization, spatial resolution and incidence angles. The Satellite has a Synthetic Aperture Radar (SAR) with multiple polarization modes, including a fully polarimetric mode in which HH, HV, VV and VH polarized data are acquired. Its highest resolution is 1 m in Spotlight mode (3 m in Ultra-Fine mode) with 100 m positional accuracy requirement. In wide scene mode the SAR has a nominal swath width of 100 km and an imaging resolution of approximately 30m [15].

The imagery used for the present study is comprised of a temporal series of 12 RADARSAT-2 wide scene images, acquired between April, 2011 and August 2012. RADARSAT wide scene images were acquired through Science and Operational Applications Research-Africa (SOAR-AF) initiative Project No. 5214. The SAR imagery were received as preprocessed level one SAR Georeferenced Fine Product (1SGF) with 25x28m resolution at an incidence angle between 20-45 degrees, with swath width of 100km. SAR imagery were analyzed and correlated with hydro climatological data on acquisition period it was observed that Five Radarsat-2 scenes were acquired during rainfall days(see Tab.1). Tab. 3 below shows the satellite imagery acquired in cross-polarized (HV) and like-polarized (VV) with dates of respective periods.

Table 3. 12 Radarsat-2 images were acquired in the Wide Swath mode (W3) and VH/VV polarization combination

Date of acquisition	Near range, θ^o	Near range ,θ^o	Image ID
30.04.2011	38.668	44.691	130941
24.05.2011	38.673	44.695	134877
02.12.2011	38.693	44.713	168386
26.12.2011	38.724	44.739	172606
19.01.2012	38.710	44.728	176536
07.03.2012	38.671	44.694	184366
31.03.2012	38.656	44.694	188688
24.04.2012	38.675	44.696	193164
18.05.2012	38.706	44.723	197548
11.06.2012	36.681	44.703	201738
05.07.2012	38.675	44.697	206020
22.08.2012	38.682	44.703	214497

3.3 Vegetation height data

Land vegetation cover was collected during an intensive field campaign conducted in September 2010. Field data were collected from 321 sites of uniform vegetated areas in the Mara wetland, floodplain and on higher terrain around the wetland floodplain area. Within the swampy wetland 75 sites were chosen due to accessibility challenges, 20 points on open water bodies, 90 points were selected on floodplain and 115 remaining points were selected around the wetland territorial areas. From each site information regarding Geographic position using a hand held Geographic Positioning System (GPS), vegetation type and average vegetation height was recorded. The common broad vegetation types in the area include herbaceous wetland vegetation, mainly papyrus sp. and Typha sp.; grasslands; shrub and thicket; forest and open water bodies [16]. The vegetation heights ranges between 0.2 for grasslands to 7m for scattered forest areas.

4.0 METHODOLOGY

4.1 Canopy height modelling and DEM correction

Different methods have been employed in estimation of vegetation canopy (height, density, biomass, LAI, NDVI) using remote sensing approach[17]-[19] and the nature of models depend on electromagnetic radiation from the sensor and target object [20]. For modeling backscatter from vegetation canopies using radar data, a common approach is to first develop direct models simulating the backscattering coefficient of a canopy with known characteristics. These models can subsequently be used in inverse mode to estimate the characteristics of vegetation canopies. The modelling approach can be grouped into three general classes which includes empirical, theoretical, and semi-empirical. An empirical model based on power law was chosen based on its simplicity and does not need a lot of variables that affect backscattering mechanism in plant canopy and ground surface as in the case of theoretical and semiemperical models [21].

The sequential procedure adapted in the analysis of data is simply described by Fig. 4 below. These included pre-processing Radarsat -2 data through terrain correction radiometric normalization[22], speckle filtering, coregistraton, staking and image subset in NESTTOOL BOX. The backscattering statistics mean and standard deviation for 12 SAR imagery was investigated. 7 SAR imagery that was observed not to be affected by flood and rainfall was also analysed separately. The selection was based on determination of Soil water Index [23], precedent aggregated rainfall and flow data. The idea was to analyse data with slightly varying dielectric constant/ soil moisture which affect backscattering mechanism.

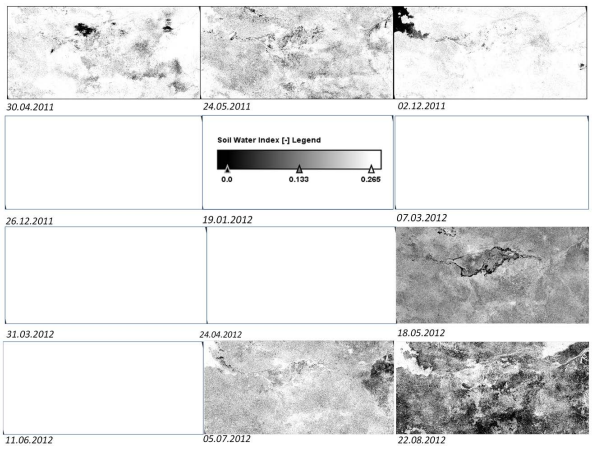

Figure 3. Images with low Soil Water Index affected by floods and rainfall

The pre-processed images were analysed statistically to determine mean, standard deviations to derive information of backscattering mechanism to aid interpretation of the effect of vegetation types, rainfall and floods on backscattering statistics. The Mean and Standard deviations were determined and exponentially correlated with vegetation heights. The best model fit was evaluated using of correlation coefficient r and coefficient of Determination R^2. The canopy height model was developed using exponential equation below based on Markov covariance theorem [24].

$$C_h = Ae^{B\sigma^o_{std}} \tag{1}$$

Where C_h is the canopy height (m); A and B are model parameters and σ^o_{std} is the standard deviation of Cross polarization or single polarisation backscatter coefficient. Where A and B represent simplification of vegetation and ground backscattering mechanism parameters respectively[24],[25].

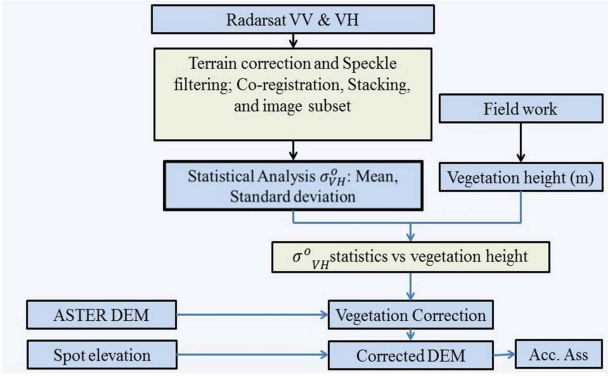

Figure 4. Topographic correction approach

The ASTER DEM was pre-processed to remove noise by using 2D Kalman filtering techniques [26], [27]. The derived Vegetation height Map was used to correct a pre-processed ASTER DEM to remove vegetation effect and the accuracy was evaluated based of root mean square error - RMSE, r and R^2.

4.2 Hydrodynamic roughness determination

SAR imagery roughness classes can be partially estimated through the ratio of VH/VV polarization channels [28]. The ratio is known as cross polarisation ratio (ρ), and it describes the back scattering mechanism within the vegetation canopy. Very high hydraulically rough surfaces and high vegetation density, therefore surface scattering mechanism dominates. This can be explained by eqn 2. The relative hydraulic roughness is a function of cross polarization ratio and incidence angle. Therefore correction of varying incidence angle can be normalised at an average of near and far incidence angle for the subset of image. For small study area as in this correction of incidence can be ignored.

$$\sigma^o_{vh} \geq \sigma^o_{vv}, \quad f(\rho,\theta) \to 1 \tag{2}$$

For sparse and less dense vegetation the cross polarisation ratio is greater than one because of the double bouncing backscattering dominates. Hence relatively lower hydraulic resistance.

$$\sigma^o_{vh} >> \sigma^o_{vv}, \quad f(\rho,\theta) \to 0 \tag{3}$$

The cross polarization ratio was inverted to obtain relative surface roughness (k_s) within a vegetation class using eqn. 4.

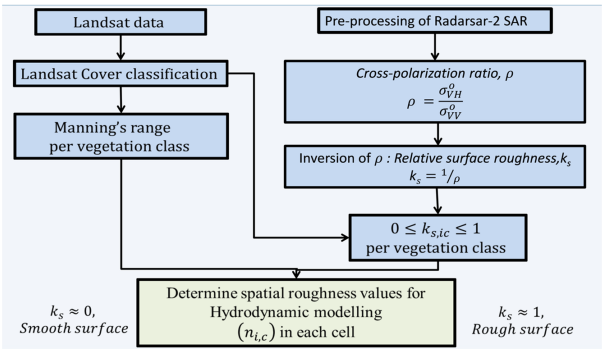

Figure 5. Hydrodynamic roughness approach

The relative surface roughness is given by the equation below.

$$k_s = \frac{1}{\rho} \quad (4)$$

Landcover classifications shape files was obtained from a previous work of the author where land use in the study area was classified as open water, swamps, open grasslands, Savannah grasslands, shrub/thicket, papyrus vegetation and forests [16].Various literature were reviewed to give guidance on selection of manning's values for each vegetation classes (Tekeregen et al., 2010; Chow,1959; O'Brien,2009; Acrement and Schneider, 1989; Bates, 2004). After careful review and investigation of manning's values by comparing the study site vegetation characteristics and those given in literature. The following manning's values range was adopted for specifying spatial roughness coefficient for the study area.

Table 3 Manning's roughness ranges for different vegetation classes [29],[32].

		Manning's coefficient, n ($m^{1/3}/s$)		
No	Vegetation/Land cover type	min $n_{min,c}$	average $n_{av,c}$	max $n_{max,c}$
1	Open water/ River bed sediment	0.02	0.05	0.085
2	Swamps	0.09	0.24	0.34
3	Open grassland	0.20	0.30	0.40
4	Savannah grassland	0.20	0.25	0.30
5	Thicket/shrub	0.30	0.35	0.40
6	Papyrus	0.17	0.49	0.80
7	Forest	0.17	0.33	0.48

Spatial hydraulic roughness was calculated by eqn. 5 below.

$$n_{i,c} = n_{min,c} + (n_{max,c} - n_{min,c}) \frac{(k_s)_{i,c} - (k_s)_{min,c}}{(k_s)_{max,c} - (k_s)_{min,c}} \quad (5)$$

where;

$n_{i,c}$ =manning's roughness value for a cell within a vegetation class

$n_{av,c}$ = mean manning's roughness value for a cell within a vegetation class

$n_{max,c}$ = maximum manning's roughness value for a cell within a vegetation class

$n_{min,c}$ = minimum manning's roughness value for a cell within a vegetation class

$(k_s)_{min,c}$ = minimum relative surface roughness value for a cell within a vegetation class

$(k_s)_{max,c}$ = maximum relative surface roughness value for a cell within a vegetation class

$(k_s)_{i,c}$ = relative surface roughness value for a cell within a vegetation class

4.3 Hydrodynamic modelling approach

FLO-2D hydrodynamic model developed by FLO-2D software INC, USA, was adapted for this study. FLO-2D is volume conservation model, which is solved with central finite difference numerical scheme formulation. It conveys the flood volume around on a series of tiles for overland flow or through stream segments for channel routing [32]. Topography and resistance control flood wave progression over the flow domain.

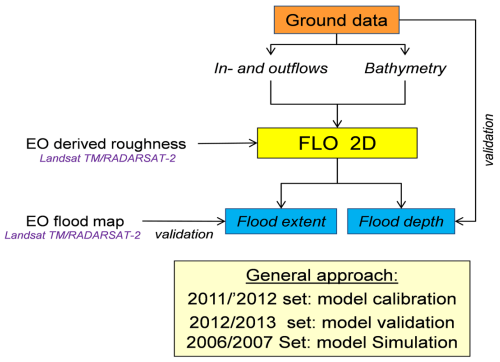

Figure 6. FLO2D modeling approach

Flood routing in two dimensions is handled through a numerical integration of the equations of motion and the conservation of flood volume. The simple volume conservation governing equations are written as general constitutive fluid equations which include continuity equation and dynamic wave momentum equation;

$$\frac{\partial y}{\partial t} + \frac{\partial hV}{\partial x} = i \quad (6)$$

$$S_f = S_o + \frac{\partial h}{\partial x} - \frac{V}{g}\frac{\partial V}{\partial x} + \frac{1}{g}\frac{dV}{\partial t} \quad (7)$$

where ***h*** is the flow depth and ***V*** is the depth-averaged velocity in one of the eight flow directions *x*. The excess rainfall intensity ***i*** may be nonzero on the flow surface. The friction slope component $\boldsymbol{S_f}$ is based on Manning's equation. The other terms include the bed slope S_o, pressure gradient and convective and local acceleration terms. This equation represents the one-dimensional depth averaged channel flow.

For the floodplain, while FLO-2D is multi-direction flow model, the equations of motion in FLO-2D are implemented by computing the average flow velocity across a grid element boundary one direction at time. There are eight potential flow directions, the four

compass directions (north, east, south and west) and the four diagonal directions (northeast, southeast, southwest and northwest). Each velocity computation is essentially one-dimensional in nature and numerically solved independently of the other seven directions. The stability of this explicit numerical scheme depends on strict criteria to control the size of the variable computational time step.

Schematic layout of the model domain is represented on Figure 7 below. The modeling was based on ground data for inflows and outflows. The Mara mine gauge station(5H2) was considered as inflows at the upstream boundary condition while the downstream boundary was considered as Lake levels. An internal gauging station height at station no.3 (Fig.7) was used for model calibration and validation. The model domain was set at 100m resolution.

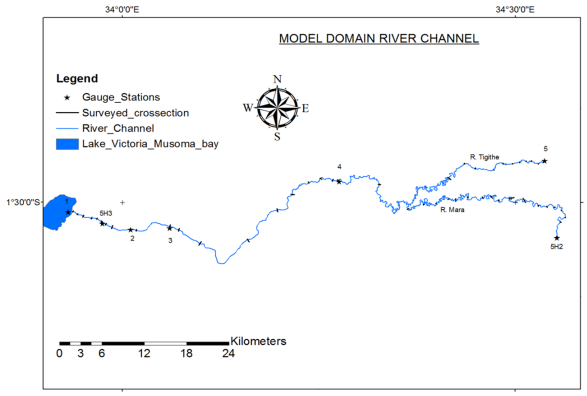

Figure 7. Schematic layout of the model domain

Calibrated ASTERDEM was used to represent the floodplain, and river channel was developed from fifty surveyed cross sections, Spatial manning's roughness was determined as explained in section 4.2 above.

5.0 RESULTS

5.1 Canopy height modelling and DEM correction

Exponential empirical equation was developed based on observed vegetation height and standard deviation of back scatter coefficient. Areas of high and low back scatter standard deviation was observed to have high and low vegetation height respectively. The correlation between cross-polarized (HV) and like-polarized (VV) backscatter coefficient and vegetation height did not yield better correlations. The standard deviation statistic of backscatter of multitemporal SAR imagery was observed to yield better correlation between canopy height. Best results were obtained by utilising seven selected imagery with no influence of rainfall and excessive floods which yield values of 0.79, 0.65 and 0.62 as correlation coefficient, standard error and coefficient of determination respectively. Therefore model No.4 was used for vegetation height correction for ASTERDEM for all areas except on grasslands and open waters.

Table 3 Canopy height model parameters

	Standard deviation Statistic	Model parameters		**r**	(SE) [dB]	R^2
No.		A	B	(r)	(SE)	R^2
1	σ^0_{vv}	5.27	-0.10	0.56	0.89	0.26
2	σ^0_{vh}	6.52	-0.15	0.63	0.81	0.39
3	σ^0_{vv7}	6.79	-2.10	0.62	0.81	0.38
4	σ^0_{vh7}	7.70	-0.27	0.79	0.65	0.62

NB: σ^0_{vh7}, σ^0_{vv7} for selected seven SAR scenes
σ^O_{vh}, σ^O_{vv} for selected all 12 SAR scenes

The accuracy assessment of raw ASTERGDEM 2 and corrected DEM is showed in Table 4. The corrected DEM yielded better statistical evaluation parameters. The comparisons were based on Mean Average Error (MAE), Root Mean Square Error (RMSE), Standard Error of Estimate(STEYX) and Coefficient of determination (R^2).

Table 4 ASTERDEM Correction statistics

Acc. statistic	Raw DEM	Corr. DEM
RMSE(m)	5.1	3.0
MAE(m)	2.4	0.4
STEYX (m)	4.6	3.94
R^2 [-]	0.83	0.90

The correction of ASTERDEM through this approach improved the elevation from RMSE of 5.1m to 3.0m while the R^2 also increased from 0.83 to 0.9.

5.2 Spatial hydraulic roughness

Spatial hydraulic roughness was determined using the concept of polarization ration for multipolarization (HV,VV) Radarsat 2 data. Copolarization ration is related to plant biomass[34]-[37]. Plant biomass is also related to resistance of flood flow in flood plain [38].

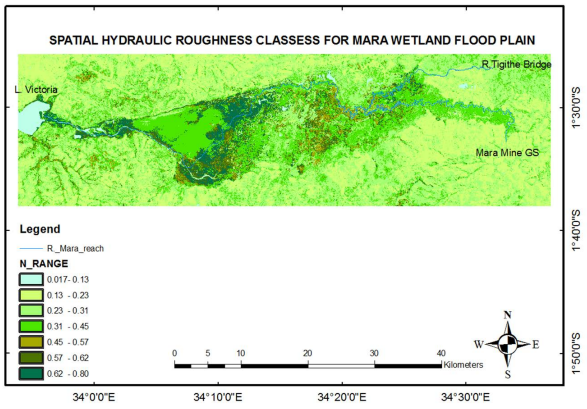

Figure 8. Spatial roughness

The hydraulic roughness of Mara floodplain and its environment ranges between 0.017 to 0.8 $m^{1/3}/s$. Open water bodies has the lowest hydraulic roughness, papyrus plants and forest has higher roughness values. Within the wetland there is heterogeneity and different plant (Papyrus) density. In the southern part along the river there is high biomass than in the northern part of papyrus wetland. This may be attributed by distribution of nutrients due to river flow. This shows that along the river channel the vegetation receives more nutrients.

5.3 Calibration and validation of hydraulic model

The model was calibrated and validated at an internal gauge station-3(Fig.7) using records for 2011 and 2012 floods events respectively, no satellite imagery was obtained to capture these flood event at peak of hydrograph. The model performance was evaluated using Index of agreement (d), Nash - Sutcliffe efficiency criterion (E), Standard error of Estimate(STEYX) and Coefficient of determination (R^2) [39]. For flood extent comparison, it was unfortunate there was no satellite data available to compare inundations derived from modeling results and Satellite data.

Table 4 Model calibration and validation results

Performance Criteria	Calibration	Validation
Index of agreement (d)	0.79	0.76
Bias (%)	12.46	14.70
Nash - Sutcliffe efficiency criterion (E)	0.38	0.45
STEYX (m)	0.24	0.52
R^2 [-]	0.71	0.67

The systematic and dynamic error present in model simulation was observed through performance criterion above. Though good values of d, R^2, the model under predicted observed flows in rising and falling limbs of flood hydrograph. Flood peaks were relatively captured which is an indicator of good model performance during flood with respect to the DEM used.

5.4 Flood modelling and ecosystem status

The Modelling results for three flood events was analysed. January 2011, May 2012 and January 2007 flood events. Table 5-7 and Figure 9-10 summarises maximum flood characteristics in the Mara wetland floodplain for three flood event scenarios.

Table 5 shows the results of flood simulation, the inundation coverage under the three flood events. For 2007, 2011 and 2012 flood events 57%, 25% and 35% of the wetland was inundated, and the total volume of surface water was 427.6, 124.7 and 195.6 million cubic meters respectively.

Table 5 Summery of Flood characteristics for each flood event

Total Area (620 km^2)	**2007**	**2011**	**2012**
Hydrograph peak discharge (m^3/s)	920	210	423
Flooded area (km^2)	352	157	218
Average depth (m)	1.2	0.8	0.89
Maximum depth (m)	4.9	4.3	4.3
Flood volume $x10^6$ (m^3)	427	124	195
Average velocity (m/s)	0.38	0.22	0.26
Maximum velocity (m/s)	2.94	2.9	3.5

Table 6 shows the maximum water depth for the three flood events. For 2007, 2011 and 2012 flood scenarios, 52.5%, 75.1% and 67.1% of the inundated area was below 1.16m. and the total volume of surface water was 427.6, 124.7 and 195.6 million cubic meters respectively. The 2007 flood event fills most of the old channels river cuts and depression in the flood plain hence increasing coverage of higher depths between 1.16-2.56m to 39.7%.

Table 6 Surface area(%) per maximum water depth class

Water depth, m	2007	2011	2012
0.01-0.56	26.4	38.0	35.2
0.56-1.16	26.1	37.1	31.9
1.16-1.79	23.1	19.1	24.2
1.79-2.56	16.6	5.6	7.7
2.56 -3.88	7.6	0.1	0.9
3.88 -5.09	0.2	0.0	0.0
5.09-9.83	0.1	0.0	0.0
Total (%)	100	100	100

Figure 9. shows areas that are flooded with greater depths are cut old channels, depressions on flood plain, and lower parts of papyrus wetland towards the lake. The simulation also reveals existence of areas that are not flooded during extreme flood events. These areas creates islands in the flood plain during flood events. Information from the local community reveals that these islands are key places for grazing animals during flood events.

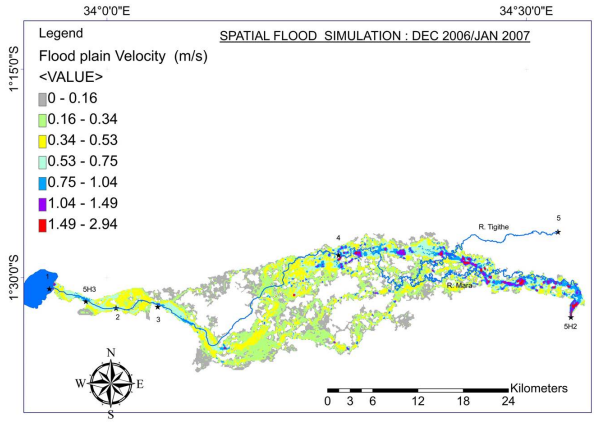

Figure 9. Spatial maximum flood depth

Table 7. shows distribution of maximum flow velocity in the floodplain for the three flood events. For 2007, 2011 and 2012 flood scenarios, 52.5%, 75.1% and 67.1% of the inundated area experience a maximum flow velocity less than 0.34m/s. For most of the inundated areas the flow velocity does not rise above 0.54m/s. The areas that experience velocity less than 0.54 m/s for 2007, 2011 and 2012 flood scenarios are 75.4%, 92.3% and 88.6%

Table 7 Surface area(%) per maximum velocity class

Water velocity, m	2007	2011	2012
0.01-0.16	24.5	49.2	41.1
0.16-0.34	28.0	26.8	31.0
0.34-0.53	22.9	16.3	16.5
0.53-0.75	14.0	4.7	7.0
0.75-1.04	6.9	2.1	2.9
1.04-1.49	2.8	0.8	1.3
1.49-2.54	0.8	0.1	0.2
2.54-3.5	0.0	0.1	0.0
Total (%)	100	100	100

The spatial maximum velocity indicate areas of high and low flow velocity. The wetland has an average slope 0.06% with average maximum velocity of 0.38m/s, 0.22m/s and 0.26m/s for 2007, 2011 and 2012 flood scenarios respectively. These low velocity indicate that this is a sediment deposition floodplain. Independent analysis of river bed and floodplain sediments indicate that deposition of sediment along the river channel has created a sediment gradient from Mara mine gauge station(5H2) to station no 4. Most of larger sand and gravel particles are deposited upstream and particle sizes decreases downstream to where most of clay and silt are deposited before water enters into dense papyrus wetland. Finer silt particles(talcum powder) always finds its way to the lake during flood events. The flood spread and deposition of sediments create a very fertile flood plain which attract agriculture activities which support livelihood of the communities around the wetland.

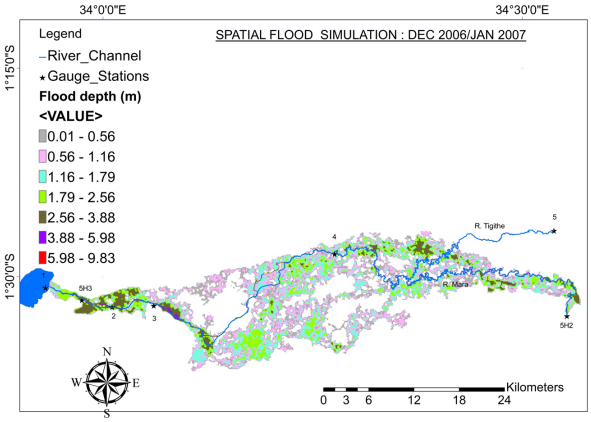

Figure 10. Spatial maximum flood velocity

6.0 DISCUSSIONS

Vegetation height derivation from standard deviation backscatter may have some limitation involved. It was observed that vegetation of height above 7m could not be captured by this concept. This may be because standard deviation of HV/VV polarization becomes insensitive to increases with biomass at a threshold level (the saturation level). The HV- polarized backscatters are found to be the most sensitive to vegetation and hence yield the highest correlations, while the VV polarized backscatter tends to saturate at lower levels of height/ biomass. These saturation points may define the upper limits for accurate estimation of vegetation height/biomass in the case of single frequency and single polarization data [36],[37]. It was observed that open grasslands vegetation was over estimated with the canopy height model. For grassland vegetation the response of backscatter is influence by geological/soil properties and moisture [40]. The higher standard deviation in canopy model parameters may be linked to heterogeneity and vegetation density in the study area.

Accuracy of topographical data was based on 731 points a combination of spot height extracted from topographic map and surveyed points within the wetland. The raw ASTERDEM was improved from RMSE of 5.1 m to 3.0 m using vegetation correction based on canopy height model developed. There is possibility of vegetation of height greater than 7m was not properly captured due to limitation of using standard deviation backscatter statistic. These areas in floodplain may increase island areas during flood modelling. Secondly, elevation points extracted from topographical maps may not actually be actual ground elevations for points that falls within the densely vegetated papyrus or flood plain forest.

During model calibration and validation, no manning's roughness optimization runs performed due to computational cost and resources available. One simulation in a 8G RAM, 2.53 GHZ computer takes about 20 days to complete one simulation. The initial model performance during calibration and validation runs. Though good model performance on index of agreement and coefficient of determination. Nash - Sutcliffe efficiency criterion was 0.38 and 0.45 with bias 12.4% and14.7% respectively during calibration and validation runs. This may be resulting from the uncertainty on quality data used for model set up. e.g. topographic data, approximations of cross-section and initialization of water levels within the model domain. Simulated water levels was relatively higher than observed water levels.

7.0 CONCLUSIONS

This study presented the initial findings of use of EO data to support hydrodynamic modelling. The use of Landsat TM in vegetation mapping, Radarsat -2 in roughness parameterization and vegetation height retrieval to support hydrodynamic model parameterization. ASTERDEM proves to be useful in 2D model parametrization for 2D hydrodynamic modelling [33].

Vegetation height model developed showed to be effective in approximating vegetation in areas of high biomass e.g. Papyrus, medium height forests and thickets. But it performed poorly in short vegetation types e.g. grasslands. Though, the spatial vegetation height derived was used to correct ASTERDEM and the accuracy improved from 0.83% to 0.9%. showing that if adequate time and resources are available detailed models for each vegetation class can be formulated to increase the accuracy of canopy height models.

The use of Radarsat-2 co-polarization ratio to derive relative surface roughness showed a good promise to facilitate spatial roughness parameterization within the model domain. The model response to peak water level at the internal gauge station gives an indication that EO data can be used qualitatively to access the hydrodynamic processes in wetlands and floodplains if accurate data is not available.

8.0 ACKOWLEGEMENTS

The author would link to thank those who supported this study. Special thanks to MaraFlows project-UNESCO-IHE and University of Dar es Salaam, Tiger Initiative Project No.24 and Tiger Initiative-AlCANTARA project No. 12-A15, ESA-SOAR Africa Program proposal No. 5126. Ministry of Water and Irrigation of the Government of Tanzania. The authors also express their thanks to all reviewers of this Manuscript.

REFERENCES

1.Bunn S.E. & Arthington A.H. (2002). Basic principles and ecological consequences of altered flow regimes for aquatic biodiversity, *Environmental Management*, 30, 492-507

2.Wande, K.M. (2010). The significance of ecosystem services in sustaining peoples livelihood; a case study in Mara wetland, Musoma and Tarime District, Tanzania. Msc. Thesis UNESCO-IHE Institute for Water Education, Delft. The Netherlands

3. GLOWS. (2007), Water Quality Baseline Assessment Report: Mara River Basin, Kenya- Tanzania. 2007. Global Water for Sustainability Program, Florida International University. 61

4.Junk W., Barley P.B. & Sparks R.E. (1989**).** The flood pulse concept in river flood plain systems. *Special publication of the Canadian Journal of Fisheries*

and Aquatic Sciences, 106, 110-127.

5.Barley P.B. (1991). The flood pulse advantage and the restoration of river systems. *Regulated Rivers: Research and Management*, 6, 75-86.

6.Junk W.,(1996) The flood pulse concept of large rivers. *Large Rivers:* 11(3).

7.Bates, P.D. & De Roo, A.P.J. (2000). A simple raster-based model for flood inundation simulation. *Journal of Hydrology.* 236 (1–2), 54–77.

8.Cobby, D.M., Mason, D.C. & Davenport, I.J. (2001). Image processing of airborne scanning laser altimetry data for improved river flood modelling. I*SPRS J. Photogram. Remote Sens.*, 56, 121–138.

9.Horritt M.S. & Bates P.D. (2002). Evaluation of 1D and 2D numerical models for predicting river flood inundation. *Journal of Hydrology.* 268, 87–99.

10.Cook, A. & Merwade, V. (2009). Effect of topographic data, geometric configuration and modeling approach on flood inundation mapping. *Journal of Hydrology*. 377(1-2), 131–142. doi:10.1016/j.jhydrol.2009.08.015.

11.Dutta, D., Alam, J., Umeda, K., Hayashi, M., & Hironaka, S. (2007). A two-dimensional hydrodynamic model for flood inundation simulation: a case study in the lower Mekong river basin. *Hydrological Processes*. 21, 1223 - 1237.

12.Di Baldassarre, G.D., Schumann, G., Bates, P.D., Freer, J.E. & Beven, K.J. (2010). Flood-plain mapping: a critical discussion of deterministic and probabilistic approaches. *Hydrol. Sci. J.*, 55, 364–376.

13.Joseph O.D. Mtamba , Preskedis M. Ndomba, Felix W. Mtalo & Allesandra Crosato.(2013). Hydraulic Study of Flood rating Curve Development in the Lower Mara Basin. Presented at 4th International Multidisciplinary Conference on Hydrology and Ecology (HydroEco 2013) May 2013, Rennes, France (unpublished).

14.Livingstone, C.E., Sikaneta, I., Gierull, C., Chiu, S. & Beaulne, P. (2005). RADARSAT-2 System and Mode Description. In Integration of Space-Based Assets within Full Spectrum Operations (pp. 15-1 – 15-22). Meeting Proceedings RTO-MP-SCI-150, Paper 15.Neuilly-sur-Seine, France: RTO. Available from: http://www.rto.nato.int/abstracts.asp.

15.MDA (2011), Radarsat-2 product description,RN-SP-52-1238, Issue 1-9

16.Joseph O.D. Mtamba, Preksedis M. Ndomba & Felix W. Mtalo (2012). Wetland Change Detection and Dynamics using Multitemporal Remote Sensing Techniques. Presented at UNESCO-IHP Conference in April 2012, Dar es Salaam (unpublished).

17.Colombo,R., Bellingeri, D., Fasolini, D. & Marino C.M., (2003). Retrival of leaf area index in different vegetation types using high resolution satellite data. *Remote Sens. Environ.* 86:120-131.

18.Ni, W., Li, X., Woodcock, C. E., Caetano, M. R. & Strahler A. H. (1999). *IEEE Trans. Geo science Rem. Sens*. 27: 1-6

19.Verrelst, J., Romijn, E. & Kooistra, L. (2012). Mapping vegetation density in heterogeneous river floodplain ecosystem using pointable CHRIS/PROBA data. *Remote Sensing.* 4(9):2866-2889.

20.Strahler, A.H. (1986). On the nature of models in Remote sensing. *Remote Sensing of Environment.* 20:121-139.

21.Bindlish, R. & Barros, P.A. (2001). Parametrization of vegetation backscatter in radar-based soil moisture extraction. *Remote Sensing of Environment.* 76:130-131.

22.Loew, A. & Mauser, W. (2007). Generation of geometrically and radiometrically terrain corrected SAR image products. *Remote Sensing of Environment.* 106:337-349.

23.Wagner,W., Guido Lemoine,G., & Rott,H. (1999b). A method for estimating soil moisture from ERS scatterometer and soil data. *Remote Sensing of Environment*, 70(2):191–207.

24. Treuhaft, R. N. & Siqueira, P. R. (2000). The Vertical Struture of Vegetated Land Surfaces from Interferometric and Polarimetric Radar, *Radio Sci.*,v35(1),141-177.

25.Mattia, F., LeoTan, T., Picard, G., Posa, F., Alessio, A., Notarnicola,C., Gatti, A.M., Rinaldi, M., Statalino, G. & Pasquariello, G. (2003a). Multitemporal C-band radar measurements on wheat fields, *IEEE Trans. Geosci. Remote Sens.* 41(7)1659-1671.

26.Wang, P. (1998). Applying two dimension kalman filtering for digital terrain modeling (Eds. D. Fritsch, M. Englich & M. Sester), IAPRS, Vol.32/4, IPRS Commission IV Symposium on GIS- Between Visions and applications, Stuttgard, Germany.

27.Gallant, J. C. & Hutchinson, M.F, (2006). Producing digital elevation models with uncertainty estimates using a multi-scale Kalman filter. 7th International Symposium on Spatial Accuracy Assessment in Natural Resources and Environmental Sciences. Accessed through http://spatialaccuracy.org/system/files/Gallant2006accuracy.pdfA

28.Paloscia, S., Pampaloni, P., Pettinato S. & Santi E, (2008), A comparison of algorithms for retrieving soil moisture from ENVISAT/ASAR images, *IEEE Trans. Geosci and Rem. Sens.*,46(10), 3274-3284.

29.Chow, V. T. (1959). Open-Channel Hydraulics, McGraw-Hill, New York, 680 pp.

30.Acrement, Jr., G. & Schneider, V. (1989). Guide for selecting manning's roughness coefficients for natural channel and floodplains. *Technical Report WSP2339*, USGS.

31.Bates, P.D. (2004). Remote sensing and flood inundation modelling. *Hydrol. Proc*., 18, 2593–2597.

32.O'Brien, J.S. (2009). Flo 2D Reference manual, FLO-2D *Inc*, Arizona, USA.

33.Tarekegn, T.H., Haile, A.H., Rientjes, T., Reggiani, P. & Alkema, D. (2010). Assessment of an ASTER-generated DEM for 2D hydrodynamic flood modeling. *Int. J. Appl. Earth Observ. Geoinf.,* doi:10.1016/j.jag.2010.05.007.

34. Dobson, M.C., Ulaby, F. T., LeToan, T., Beandoin, A. and Kasisehke, E. S. (1992b). Dependence of radar backscatter on conifer forest biomass, *IEEE Trans. Geosci. Remote Sens.* 30(2),412-415.

35.Ranson K.J. & Sun, G. (1994). Mapping biomass of a northern forest using multifrequency SAR data, *IEEE Trans. Geosci. Remote Sens.* 32:388-396.

36. Dobson, M.C., Ulaby, F. T., LeToan, T., Pierce L.E., Sharik T.L., Bergen K.M., Kellndorfer, J., Kendra, J R., Li, E., Lin, Y.C., Nashashibi, A., Sarabandi, K., & Siqueira, P. (1995). Estimation of forest biophyisical characteristics in Northern Michigan with SIR-C/X-SAR. *IEEE Trans. Geosci. Remote Sens.* 33:877-895.

37.Imhoff, M.L. (1995). Radar backscatter and biomass saturation: ramifications for global biomass inventory, *IEEE Trans. Geosci. Remote Sens.* 33(2), 511-518.

38.De Donker, L., Troch,P., Verhoeven, R., Bal,K., Meire,P. & Quintelier, J., (2009). Determination of the Manning roughness coefficient influenced by vegetation in the river Aa and Biebrza river. *Environ. Fluid Mech*, 9, 549-567.

39.Krause, P., Boyle, D.P., & Base, F. (2005). Comparision of different effeciency crireria for hydrological model assessment, *Advances in Geosciences,*5, 89-97. SRef-ID: 680-7359/adgeo/2005-5-89.

40 Wang ,Y., Kasischke, E. S., Melack, J. M., Davis, F.W. & Christensen(Jr.), N. L. (1994), The effects of changes in loblolly pine biomass and soil moisture on ERS-1 SAR backscatter. *Remote Sensing of Environment.* 49:1:25-35.